To eat and not be eaten: Optimal foraging behavior in suspension feeding copepods.

Thomas Kiørboe[a] & Houshuo Jiang[b]

[a]Centre for Ocean Life, National Institute for Aquatic Resources, Technical University of Denmark, Kavalergården 6, 2920 Charlottenlund, Denmark; and [b]Department of Applied Ocean Physics and Engineering, Woods Hole Oceanographic Institution, Woods Hole, MA 02543, USA.

Running head: Optimal foraging in zooplankton

Corresponding author: Thomas Kiørboe, tk@aqua.dtu.dk; Tel: +45 3588 3401; Cell: +45 4011 1884; Fax: +45 3588 3434

Abstract

Zooplankton feed on microscopic prey that they entrain in a feeding current or encounter as they cruise through the water. They generate fluid disturbances as they feed and move, thus elevating their risk of being detected and encountered by predators. Different feeding modes generate different hydrodynamic signals to predators and different predator encounter speeds but may also differ in their efficiency; the optimal behavior is that which maximizes the net energy gain over the predation risk. Here, we show by means of flow visualization and simple hydrodynamic and optimization models that copepods with a diversity of feeding behaviors converge on optimal, size-independent specific clearance rates that are consistent with observed clearance rates of zooplankton, irrespective of feeding mode, species and size. We also predict magnitudes and size-scaling of swimming speeds that are consistent with observations. The rationalization of the magnitude and scaling of the clearance rates of zooplankton makes it more suitable for development of models of marine ecosystems, and is in particular relevant in predicting the size structure and biomass of pelagic communities.

Key words: Zooplankton fluid dynamics; Mortality risk; Optimal foraging; Copepod; *Centropages typicus*; *Temora longicornis*.

INTRODUCTION

Marine zooplankton are the principal consumers of the oceans' primary production. They feed in a viscous and nutritionally dilute environment and they must daily clear an enormous volume of water of prey to cover their needs. The maximum clearance rate of zooplankton varies substantially between species, but it scales with body mass when considered over the entire size, taxonomic, and feeding type range of zooplankton, from heterotrophic flagellates a few micrometers long to centimeter sized krill, and the specific clearance rates scatter around a value corresponding to ~10^6 times their own body volume per day (Hansen *et al.* 1997, Kiørboe 2011). However, feeding not only leads to acquisition of food but also involves an elevated mortality risk because feeding and swimming generate hydrodynamic disturbances that may be perceived by rheotactic predators (Gallager 1993), and motility increases encounter velocities (Evans 1989). Different feeding modes imply different risks but may also differ in efficiency in terms of volume of water cleared. For example, passive ambush feeding creates minimal fluid signals and predator encounter velocities but is inherently less efficient than the more active but 'noisy' feeding strategies of generating a feeding current or cruising through the water to hunt for prey (Kiørboe *et al.* 2010, Jiang & Kiørboe 2011). The optimal foraging strategy is that which maximizes the clearance rate or energy gain over the mortality risk. Thus, the trade-offs associated with the 3 principal feeding behaviors of zooplankton – ambush feeding, feeding-current feeding (hovering), and cruise feeding – determine the optimal feeding strategy and the magnitude and scaling of the clearance rate (Lima & Dill 1990, Visser 2007, Visser *et al.* 2009, Kiørboe 2011). The magnitude of the clearance rate of zooplankton cannot be explained by its sufficiency to maintain a population because natural selection operates at the level of the individual. The question

of what governs the magnitude of the clearance rate may be addressed, however, by quantifying the trade-offs and determining the behavior that optimizes these trade-offs.

Here, we attempt to quantify the trade-offs and determine the optimal foraging strategies and resulting clearance rates for zooplankton. We consider only the two active feeding modes since ambush feeding is restricted to a few groups of zooplankton (Kiørboe 2011). The clearance rate is determined by the flow of water past the animal and by its ability to remotely detect and capture prey. The feeding-dependent mortality risk is governed by the fluid disturbances that the animal produce that make it detectable by rheotactic predators, and by the velocity at which it translates through the water that influences the encounter rate with predators irrespective of their sensory modes (rheotactic, visual, or tactic).

Hydrodynamics of swimming and feeding in zooplankters are rather well understood, both through observations and flow visualization (Tiselius & Jonsson 1990, Malkiel *et al.* 2003, Catton *et al.* 2007, Leptos *et al.* 2009) and by means of fluid dynamical models (Lighthill 1975, Tiselius & Jonsson 1990, Visser 2001, Jiang *et al.* 2002a,b). The simplest analytical models to describe zooplankton feeding consider either a hovering zooplankter that generates a feeding current, or a neutrally buoyant one that cruises through the water. Far-field flow fields generated by these behaviors are traditionally approximated by, respectively, a stokeslet, i.e., a stationary downward-directed force that works in a point in the water and exactly balances the gravitational force acting on the animal; or a stresslet, two oppositely directed forces of equal magnitude corresponding to the propulsion force that drives the animal through the water and counterbalances the oppositely directed drag force (Fig. 1, Visser 2001). One conclusion from such simple models is that not only do the imposed flow fields differ significantly, making the hovering feeding mode the more efficient of the two (Lighthill 1975); the hovering zooplankter also generates a fluid signal that extends much further

in the water than that generated by the cruising one, thus exposing it to a greater predation risk. This conclusion is generally supported by observations of copepods (Tiselius & Jonsson 1990, Catton *et al.* 2007) and microorganisms (Glud & Fenchel 1999, Christensen-Dalsgaard & Fenchel 2003). Real zooplankters, however, are neither exactly neutrally buoyant nor apply a force that exactly balances gravity. Rather, most are negatively buoyant, so part of the force generated by the vibrating appendages or cilia goes into countering gravity and generating a feeding current and part into translating the zooplankter through the water. The resulting far-field flow may be described by the sum of a stokeslet and a stresslet (Jiang *et al.* 2002a, Fig. 1). This idealized model describes the entire range of active feeding behaviors, from pure hovering to pure cruising and, importantly, it quantifies the associated trade-offs, i.e., the clearance rate from which the animal gains food, and the translation velocity and fluid disturbance that together govern the risk of feeding.

Here we use flow visualization of feeding zooplankters and simple stokeslet-stresslet and optimization models. We show that optimal foraging is consistent with the entire range of feeding behaviors reported for zooplankton and that it predicts specific clearance within the range observed. As study object we use planktonic copepods, the absolutely dominating mesozooplankton group in the ocean (Humes 1994).

MATERIAL AND METHODS

Experiments

Late copepodids and adults of two species of copepods, *Temora longicornis* (prosome length 0.5 – 1.0 mm) and *Centropages typicus* (0.9 – 1.3 mm), were collected from a pier in Woods Hole, Massachusetts, USA, at ~5 ^{0}C and acclimated overnight at room temperature (~20 ^{0}C). Observations were made in small aquaria (65-200 ml) containing 5-10 copepods, flagellates and diatoms (to stimulate feeding) and 5 μm neutrally

buoyant beads to visualize the flow. The flow generated by feeding copepods was visualized using Particle Image Velocimetry (PIV). A red, vertically oriented laser sheet (1 W, 1 mm thick) was directed into the aquarium to illuminate the beads occurring in a well defined plane. We filmed through a dissecting microscope oriented perpendicular to the laser sheet using a high-resolution (1024×1024 pixels) Photron Fastcam 1024 PCI camera with a field of view of 8.24×8.24 mm^2. Recordings were made at 500 Hz and sequences of feeding copepods swimming in the illuminated plane were analyzed at 250 Hz, with standard PIV software (DaVis 8, LaVision) to yield flow fields.

We analyzed 12 sequences for *T. longicornis* and 11 for C. *typicus* (all different individuals). Sequences varied in duration between 500 and 3000 ms. The animal itself was excluded from the PIV analysis by masking it. The areas (excl. the animal) within which the imposed fluid velocity exceeded threshold values, U^*, were measured using ImageJ software for set values of U^* between 0.1 – 3.0 mm s^{-1}. For U^* exceeding the translation velocity of the copepod, the cross-sectional area of the copepod was added to estimate the *area of influence, S*. This area is of interest because the flow component that a rheotactic predator perceives is the velocity generated by the prey (Visser 2001). *S* is therefore the encounter cross section of the zooplankter towards a rheotactic predator with a threshold velocity for detection, U^*. Animal translation velocities, frequencies of appendage vibration as well as the size (prosome length) of the animals were measured on the videos. The average translation velocity and flow velocities were computed for periods when the flow field had developed fully after onset of swimming.

Model

We model a hovering zooplankter as a stokeslet, a neutrally buoyant, cruising zooplankter as a stresslet, and we combine the stresslet and stokeslet models to describe the feeding or swimming current of a negatively buoyant, swimming zooplankter (Fig. 1). The models assume low Reynolds numbers, and we utilize that flow components are

additive at low Reynolds numbers. Equation derivations are given in the electronic supplementary material, Appendix A1. For both models we derive explicit equations for the area of influence, S; for the combined model it can only be calculated numerically. We estimate the zooplankter's clearance rate (Ω) as the flux of water through a circle oriented perpendicular to the direction of the applied force(s) and with its center in the application point of the stokeslet or the center of the stresslet. The radius of this circle is the sensory distance or encounter radius of the zooplankter. The model thus assumes that all prey passing within the sensory or encounter radius are captured and hence provides an upper limit.

Optimal foraging

The contribution of a particular foraging behavior to the fitness of an organism can be approximated by the ratio of the net gain over the risk associated that behavior (Visser *et al.* 2009, Gilliam & Fraser 1987, Houston *et al.* 1993). The optimal foraging behavior is that which maximizes this ratio. Specifically, we define a dimensionless foraging index, χ, as:

$$\chi = \frac{\Omega - \Omega'}{E + E_0},$$

where Ω' (L^3T^{-1}) is the overhead clearance rate covering basal metabolism and costs of swimming and generating a feeding current, E is the volumetric predator-specific encounter rate (L^3T^{-1}), and E_0 is the background mortality normalized by the concentration of predators. E depends on the type of predators present; for rheotactic predators, $E=S(v^2+u^2)^{1/2}$ and for visual and tactic predators, $E=\pi R^2(v^2+u^2)^{1/2}$, where v is the velocity of the predator and R is the detection radius of the predator. Parameterization of the foraging index is described in the electronic supplementary material, appendix A1.

RESULTS

We recorded the fluid flow generated by two free-swimming copepods, *Temora longicornis* and *Centropages typicus*. *T. longicornis* (0.5-1.0 mm prosome length) vibrates its feeding appendages more or less continuously at a frequency of 28 ± 4 Hz, generating a rather constant feeding current that extends a few body lengths away from the animal (Fig. 2). The animal also translates slowly through the water at a speed (1-5 body lengths s^{-1}) and direction that depends on the orientation of the animal. The individual shown in Fig. 2 moves horizontally, from right to left, i.e., more or less backwards. The well-defined feeding current pulls in water from above and generates a posteriorly and mainly downward directed jet away from the animal.

The velocity of the imposed fluid flow attenuates with increasing distance to the copepod, and the area of influence (S) therefore declines with increasing threshold velocity, U^*. The magnitude of this area, and its scaling with U^*, is quite well described by the combined stokeslet-stresslet model (Fig. 3 A-C).

Centropages typicus (0.9-1.3 mm prosome length) has short feeding bouts, interrupted by sinking events. Feeding and sinking events are of variable but approximately equal durations, 100-500 ms. During feeding bouts the animal vibrates its feeding appendages at a significantly higher frequency than *T. longicornis* (43 ± 5 vs. 28 ± 5 Hz; $P < 0.001$), and *C. typicus* also translates through the water at a much higher speed (5.5 ± 1.7 vs. 3.0 ± 1.5 BL s^{-1}; $P = 0.001$). During feeding bouts the animal produces a backward-directed jet (Fig. 2B). The backward jet of *C. typicus* is more pronounced than that produced by *T. longicornis*, but its feeding current is much less defined. The spatial structure of the flow field for the example shown in Fig. 2B is roughly approximated by that predicted from the combined stokeslet-stresslet model for the same event in Fig. 1, i.e., asymmetric.

The flow field generated by *C. typicus* fluctuates with the activity (swimming-sinking) of the animal, but the response is not immediate: The area of influence increases for some time after the onset of the vibration of the feeding appendages; similarly, after cessation of appendage movements, the area of influence attenuates over some time. For example, it takes about 300 ms for S ($U^* = 0.6$ mm s^{-1}) to stabilize. This time scale may be compared to the viscous time scale (S/viscosity), which is of the order of 1 s for $S \sim 1$ mm^2. For smaller values of U^*, the area of influence increases, and the temporal variation in the extension of the flow field declines. Hence, at further distances, the signal perceived by a predator becomes more temporally uniform. The extension and dependency of U^* of the stabilized area of influence are again well approximated by the combined stokeslet-stresslet model (Fig. 3 D-F).

DISCUSSION

The simple stokeslet-stresslet model captures essential features of the observed flow fields generated by two copepod species with rather different behaviors, i.e., one near hovering and with a rather well developed feeding current (*T. longicornis*), and one that cruises relatively fast through the water and has a less well developed feeding current (*C. typicus*). The spatial extension of the flow field is of the same magnitude as that predicted (Fig. 2, 3). The observed scaling of the area of influence (S) with the threshold velocity (U^*) appears to deviate slightly but systematically from that predicted, having a slightly steeper slope. The main reason for the slower-than-anticipated spatial attenuation of the flow is likely to be the unavoidable background convection in the observation aquaria. However, the overall fair correspondence warrants using this idealized model to evaluate the trade-offs associated with the hovering, cruising, and intermediate behaviors. The trade-offs are in the magnitude of the clearance rate (Ω), the area of influence (S), and the swimming velocity (u) that together determine the fitness-contribution of the behavior, as defined by the foraging index, χ.

Feeding behavior and the fitness contribution of the feeding behavior so defined are solely functions of the magnitude of the force that the zooplankter generates and of its excess density ($\Delta\rho$). Both are under partial control of the animal on an evolutionary time scale, and we can therefore construct landscapes of the foraging index within this parameter space (Fig. 4). The diagonal in these plots corresponds to the force exactly balancing gravity: the zooplankter is hovering. Below this line, the animal produces a feeding current *and* translates through the water, the faster the further away from the diagonal. At $\Delta\rho = 0$ the zooplankter is a 'pure' cruiser with no feeding current.

In the presence of visual or tactile predators only (Fig. 4A-C), the global optimum of the foraging index landscape suggests that the zooplankter should be hovering and be very heavy and generate a correspondingly large force. However, there is a limit to how much muscle force a zooplankter can produce and how heavy it can be, and the optimal strategy depends on whether the zooplankter is limited by its density or by the force it can produce (Fig. 4A-F). The maximum mass-specific net force output of muscle motors is strikingly constant across all animal taxa, including both vertebrates and invertebrates, it is limited by material fatigue rather than power production, and it averages a temperature-independent value of 57 N kg^{-1} muscle (Marden 2005, Marden & Allen 2002). Assuming that 20 % of the copepod volume is muscle (Lenz *et al.* 2004), this corresponds to about 10^4 N m^{-3}. Mass-specific force output of ciliary motors may be higher (Marden 2005). If force rather than excess density is the limiting factor, hovering should always be the preferred strategy independent of organism size if visual and tactic predators dominate (Fig. 4A-C).

The limit to how dense a zooplankter can be, however, typically defines a more narrow constraint. Excess densities of most zooplankters, evaluated from direct measurements or from sinking speeds, are <30 kg m^{-3} - from ciliates to copepods and including even larvae of echinoderms with calcified skeletons (Knutsen *et al.* 2001, Dunham & Child

1961, Pennington & Strathman 1990). Only shelled forms, such as bivalve larvae and pteropods (wing snails), have much higher densities, ~ 100 kg m^{-3} (Davenport & Bebbington 1990, Wildish & Kristmanson 1997). There are obvious disadvantages to a high excess density; there are costs of maintaining ion pumps and depositing ballast (Visser *et al.* 2009), and a high density hampers rapid escape jumps, essential for predator avoidance in many zooplankters, from flagellates and ciliates to copepods (Jakobsen 2001, Buskey *et al.* 2002). With density as the limiting factor, there is a clear optimum in the foraging index landscape that depends on the excess density that the zooplankter can achieve (Fig. 4A-C). The optimum force production and the resulting specific clearance rate are both largely invariant with density, and the optimum specific clearance is ~10^6 d^{-1}. The optimum swimming velocity depends on the excess density (the denser and slower the better) but the predicted magnitudes are comparable with those observed for zooplankters of this size (Fig. 5) and realized by the experimental organisms examined here.

In the presence of only rheotactic predators, or for zooplankters too small to be detected by vision and where hydrodynamic perception are more important, there is a global optimum in the foraging index landscape within the likely constraints set by density and force production, at least for intermediately sized zooplankters (Fig. 4D-F). The predicted specific clearance rate at the optimum is similar to that predicted above, i.e., of order 10^6 d^{-1}. Again the predicted strategy changes if the optimum excess density or force is unachievable and depends on whether one or the other is limiting. If force is the limiting factor, the optimum strategy is either hovering at low forces, or slow swimming with higher forces, and the optimum density is < 100 kg m^{-3}, consistent with observations. The predicted swimming velocities are of the same order as for tactile and visual predation (Fig. 5).

Zooplankters may overcome limitations caused by low excess density in various ways: they may attach to solid surfaces such as those provided by marine snow and utilized by some flagellates (Fukuda & Koike 2000); they may increase their drag by attaching to particles as reported for some free-living flagellates (Christensen-Dalsgaard & Fenchel 2003) or by producing mucus strings such as done by some bivalve larvae (Fenchel & Ockelmann 2002); or they can otherwise be equipped with 'drift anchors', such as some copepods that have long, plumose appendages (Kiørboe 2011). These are common strategies that can be readily understood in the foraging optimization framework.

While the predicted optimum strategy is sensitive to the choice of parameters and underlying assumptions, the magnitude of the optimum specific clearance rate is not; even order-of-magnitude variation in input parameters leads to rather small changes in predicted specific clearance rate that remains of order 10^6 - 10^7 d^{-1} and within the range observed (Table 1). Even if we make the extreme assumption that there are no metabolic costs and no background mortality (i.e., $\Omega' = 0$ and $E_0 = 0$) then for realistic excess densities (say, 5 kg m^{-3}) the predicted clearance rates are within a factor of 5 of those predicted for default parameters, and well within the range observed (Fig. 5).

Our model considers the feeding behaviors that are hardwired in the genes of the zooplankter and, hence, the potential clearance rates that are adapted to the general environment. This is the clearance rate that one can measure at non-saturating concentrations in an experimental bottle, and these are the rates taken from the literature and to which we compare our predictions (Fig. 5, Hansen *et al.* 1997, Kiørboe 2011). Obviously, zooplankton may in addition adapt behaviorally on short time scale to their immediate environment, and realized clearance rates may therefore be lower due to food saturation or presence of predators (Visser 2007).

While we have used copepods as model organisms in this study, our results may apply more generally to marine zooplankton, because the present categorization of feeding behaviors applies to other zooplankters as well (Kiørboe 2011). However, the model is invalid for some very small zooplankters that operate at low Péclet numbers, where diffusion rather than advection governs prey encounter (Langlois *et al.* 2009), and for the largest zooplankters (krill, jellyfish), where the assumption of low Reynolds number is violated.

Sensitivity of the predicted feeding behavior to changes in parameter values and in particular to variation in the excess density that a zooplankter can achieve may account for the huge diversity in feeding behaviors that one can observe in nature. Copepod feeding behaviors, for example, range from very nearly hovering to very fast cruising with velocities of > 10 body lengths s^{-1}, and cruising and hovering may even be found within the same species (Tiselius & Jonsson 1990, Mazzocchi & Paffenhöfer 1999). The same range of behaviors is found among small zooplankters that may swim fast (10-100 body lengths s^{-1}; Hansen *et al.* 1997), or 'pseudohover' by attaching to surfaces.

While our model predicts rather well the central tendency in the observations of clearance rates and swimming velocities over a 6 order-of-magnitude range in individual biomasses and for very diverse zooplankters, there is substantial variability in the observations of in particular specific clearance rates (Fig. 5). This variability may be explained by factors that are not accounted for in our simple model. Higher clearance rates may be due to a number of potential mechanisms: zooplankters may hide from rheotactic predators in turbulence and hence can afford a stronger fluid signal, and turbulence may lead to behavior-independent increases in both predator- and prey contact rates (Rothschild & Osborne 1984), all leading to higher optimum clearance rates. Predators may be selective and zooplankters may escape predators, which imply

that predation mortality rate is less than predator encounter rate and thus allows for a more risky zooplankton behavior. Lower zooplankton clearance rates may similarly be predicted if zooplankters are selective and if their prey can escape or defend themselves (e.g. spines), or if the zooplankton predators are mainly visual ambush feeders. In general, different species of copepods and zooplankton may be adapted to different environments and possess defense and sensory capabilities as indicated above, which together may account for the substantial scatter in clearance rates observed between species.

The magnitude of the zooplankton clearance rate has interest on its own as it governs the growth, reproduction and entire bioenergetics of the individuals. However, it also has implications for properties of the ecosystem: the biomass – not the productivity – of planktonic ecosystems is inversely related to the magnitude of the clearance rate of the zooplankton. This result follows both from ecosystem size spectra theory (Andersen & Beyer 2006) and from simple predator-prey models, such as Lotka-Volterra: the biomass of both predators and prey are inversely related to the magnitude of the predator's clearance rate (Pielou 1969). Thus, the biomass of planktonic ecosystems is a property that partly emerges from interactions between individuals that, in turn, are governed by natural selection.

ACKNOWLEDGMENT. The work was supported by grants from the Danish Council for Independent Research, The Niels Bohr Foundation, and The Carlsberg Foundation to TK, and by grants from the U.S. National Science Foundation to HJ (NSF OCE-1129496 and ISO-0718506).

References

Andersen, K.H. & Beyer, J.E. 2006 Asymptotic size determines species abundance in the marine size spectrum. *Am. Nat.* **168**, 54-61. (doi: 10.1086/504849)

Buskey, E.J., Lenz, P.H. & Hartline, D.K. 2002 Escape behavior of planktonic copepods in response to hydrodynamic disturbances: High-speed video analysis. *Mar. Ecol. Prog. Ser.* **235**, 135–146. (doi: 10.3354/meps235135)

Catton, K.B., Webster, D.R., Brown, J. & Yen, J. 2007 Quantitative analysis of tethered and free-swimming copepodid flow fields. *J. Exp. Biol.* **210**, 299–310. (doi:10.1242/jeb.02633)

Christensen-Dalsgaard, K.K. & Fenchel, T. 2003 Increased filtration efficiency of attached compared to free-swimming flagellates. *Aquat. Microb. Ecol.* **33**, 77-86. (doi:10.3354/ame033077)

Davenport, J. & Bebbington, A. 1990 Observations on the swimming and buoyancy of some cosomatous pteropod gastropods. *J. Mollus. Stud.* **56**, 487-497.

Dunham, P.B. & Child, F.M. 1961 Ion regulation in *Tetrahymena*. *Biol. Bull.* **121**, 129-40.

Evans, G.T. 1989 The encounter speed of moving predator and prey. *J. Plankton Res.* **11**, 415-417.

Fenchel, T. & Ockelmann, K.W. 2002 Larva on a string. *Ophelia* **56**, 171-178.

Fukuda, H. & Koike, I. 2000 Feeding currents of particle-attached nanoflagellates—a novel mechanism for aggregation of submicron particles. *Mar. Ecol. Prog. Ser.* **202**, 101–112. (doi:10.3354/meps202101)

Gallager, S.M. 1993 Hydrodynamic disturbances produced by small zooplankton: case study for the veliger larva of a bivalve mollusk. *J. Plankton Res.* **15**, 1277-1296.

Gilliam, J.F. & Fraser, D.F. 1987 Habitat selection under predation hazard: test of a model with stream-dwelling minnows. *Ecology* **68**, 1856–1862. (doi:10.2307/1939877)

Glud, R.N. & Fenchel, T. 1999 The importance of ciliates for interstitial solute transport in benthic communities. *Mar. Ecol. Prog. Ser.* **186**, 87-93. (doi:10.3354/meps186087)

Hansen, P.J., Bjørnsen, P.K. & Hansen, B.W. 1997 Zooplankton grazing and growth: scaling within the 2-2,000-µm body size range. *Limnol. Oceanogr.* **42**, 687-704.

Houston, A.I., McNamara, J.M. & Hutchinson, J.M.C. 1993 General results concerning the trade-off between gaining energy and avoiding predation. *Phil. Trans. R. Soc. Lond. B* **341**, 375–397. (doi:10.1098/rstb.1993.0123)

Humes, A.G. (1994). How many copepods? *Hydrobiologia,* 292/293, 1–7.

Jakobsen, H.H. 2001 Escape response of planktonic protists to fluid mechanical signals. *Mar. Ecol. Prog. Ser.* **214**, 67-78. (doi:10.3354/meps214067)

Jiang, H., Osborn, T.R. & Meneveau, C. 2002a The flow field around a freely swimming copepod in steady motion: Part I theoretical analysis. *J. Plankton Res.,* **24**, 167-189. (doi: 10.1093/plankt/24.3.167)

Jiang, H., Meneveau, C. & Osborn, T.R. 2002b The flow field around a freely swimming copepod in steady motion: Part II numerical simulation. *J. Plankton Res.* **24**, 191-213. (doi:10.1093/plankt/24.3.191)

Jiang, H. & Kiørboe, T. 2011 The fluid dynamics of swimming by jumps in copepods. *J. Roy. Soc. Interface* **8**, 1090-1103. (doi:10.1098/rsif.2010.0481)

Kiørboe, T. 2011 How zooplankton feed. Mechanisms, traits and trade-offs. *Biol. Rev.* **86**, 311–339. (doi:10.1111/j.1469-185X.2010.00148.x)

Kiørboe, T., Jiang, H. & Colin, S.P. 2010 Danger of zooplankton feeding: The fluid signal generated by ambush feeding copepods. *Proc. Ro. Soc. B* **277**, 3229-3237. (doi:10.1098/rspb.2010.0629)

Knutsen, T., Melle, W. & Calise, L. 2001 Determining the mass density of marine copepods and their eggs with a critical focus on some previously used methods. *J. Plankton Res.* **23**, 859-873. (DOI: 10.1093/plankt/23.8.859)

Langlois, V., Andersen, A., Bohr, T., Visser, A. & Kiørboe, T. 2009 Significance of swimming and feeding currents for nutrient uptake in osmotrophic and interception feeding flagellates. *Aquat. Microbiol.* **54**, 35-44. (doi: 10.3354/ame01253)

Lenz, P.H., Hower, A.E. & Hartline, D.K. 2004 Force production during pereiopod power strokes in *Calanus finmarchicus*. *J. Mar. Syst.* **49**, 133–144. (doi:10.1016/j.jmarsys.2003.05.006

Leptos, K.C., Guasto, J.S., Gollub, J.P., Pesci, A.I. & Goldstein, R.E. 2009 Dynamics of Enhanced Tracer Diffusion in Suspensions of Swimming Eukaryotic Microorganisms. *Phys. Rev. Lett.* **103**, 198103.(doi:10.1103/PhysRevLett.103.198103)

Lighthill, J. 1975 Flagellar hydrodynamics. *SIAM Review* **18**, 161–230.

Lima, S. & Dill, L.M. 1990 Behavioral decisions made under the risk of predation: a review and prospectus. *Can. J. Zool.* **68**, 619–640. (doi: 10.1139/z90-092)

Malkiel, E., Sheng, I., Katz, J. & Strickler, J.R. 2003 The three-dimensional flow field generated by a feeding calanoid copepod measured using digital holography. *J. Exp. Biol.* **206**, 3657–3666. (DOI: 10.1242/jeb.00586)

Marden, J.H. 2005 Scaling of maximum net force output by motors used for locomotion. *J. Exp. Biol.* **208**, 1653–1664. (doi: 10.1242/jeb.01483)

Marden, J.H. & Allen, L.R. 2002 Molecules, muscles, and machines: universal performance characteristics of motors. *Proc. Natl. Acad. Sci. USA* **99**, 4162–4166. (doi:10.1073/pnas.022052899)

Mazzocchi, M.G. & Paffenhöfer, G.A. 1999 Swimming and feeding behaviour of the planktonic copepod *Clausocalanus furcatus*. *J. Plankton Res.* **21**, 1501-1518. (doi: 10.1093/plankt/21.8.1501)

Pennington, J.T. & Strathman, R.R. 1990 Consequences of the calcite skeletons of planktonic echinoderm larvae for orientation, swimming, and shape. *Biol. Bull.* **179**, 121-133.

Pielou, E.C. 1969 *An Introduction to Mathematical Ecology*. New York: Wiley-Interscience.

Rothschild, B. R. & Osborn, T. R. 1988 Small-scale turbulence and plankton contact rates. *J. Plankton Res.* **10**, 465-474

Tiselius, P. & Jonsson, P.R. 1990 Foraging behavior of 6 species of calanoid copepods – observations and hydrodynamic analysis. *Mar. Ecol. Prog. Ser.* **66**, 23-33.

Visser, A.W. 2001 Hydromechanical signals in the plankton. *Mar. Ecol. Prog. Ser.* **222**, 1-24. (doi:10.3354/meps222001)

Visser, A.W. 2007 Motility of zooplankton: fitness, foraging and predation. *J. Plankton Res.* **29**, 447-461. (doi:10.1093/plankt/fbm029)

Visser, A.W., Mariani, P. & Pigolotti, S. 2009 Swimming in turbulence: zooplankton fitness in terms of foraging efficiency and predation risk. *J. Plankton Res.* **31**, 121-133. (doi:10.1093/plankt/fbn109)

Wildish, D.J. & Kristmanson, D.D. 1997 *Benthic Suspension Feeders and Flow*. Cambridge University Press, Cambridge, United Kingdom.

Legends for figures

Figure 1. Illustration of the three simple models used to describe (A, D) a hovering zooplankter (stokeslet), (B, E) a cruising zooplankter that is neutrally buoyant (stresslet), and (C, F) a cruising zooplankter that is negatively buoyant (stokeslet + stresslet). The upper panels show the forces acting on the water (as vectors) and the lower panels the velocity contour lines superimposed on flow velocity vectors for the three models. The forces acting on the water due to a hovering and a cruising zooplankter are described in the text. The negatively buoyant cruising zooplankter acts with three forces on the water (C), one downward force to counter gravity (the stokeslet component), and two forces corresponding to the propulsion and drag forces (the stresslet component). The flow velocity at any point in space in the combined model is simply the sum of velocity contributions from the stokeslet and the stresslet components. The cruising zooplankter swims at velocity **U**, the stokeslet is of the point-force magnitude W_{excess} (the zooplankter's excess weight), and the stresslet of intensity $6\pi\mu a_e|\mathbf{U}|\times 2a_e$. The calculation example uses parameters for the *Centropages typicus* shown in Fig. 3B.

Figure 2. Examples of instantaneous flow fields of feeding *Temora longicornis* (A) and *Centropages typicus* (B). Regions with flow velocities exceeding $U^* = 0.6$ mm s^{-1} are shaded white.

Figure 3. Examples of observed and modeled magnitude of 'area of influence', S, as a function of the threshold velocity, U^*. A-C are *Temora longicornis*; D-E are *Centropages typicus*. L and u are prosome length and swimming speed, respectively.

Fig 4. Landscapes of the foraging index for 3 sizes of zooplankters in the presence of visual/tactile predators (A-C) or rheotactic predators (D-F) and optimum swimming velocities ($u_{optimal}$) as a function of excess density ($\Delta\rho$) of the zooplankter (G-I). The landscapes are contoured in the parameter space of the excess density of the zooplankter and the body-volume specific force that it produces (f^*). Black lines in (A-F) are contour lines for body-volume specific clearance rates (x 10^6 d^{-1}). Purple and blue lines in (A-F) describe the optimum foraging behavior when, respectively, force production or excess density limits the performance of the zooplankter. We used $V = 0.059\ L^3$ to convert between body length (L) and body volume (V)

Figure 5. Comparisons of observed and predicted clearance rates and swimming speeds of zooplankton. All observed values are those compiled by Kiørboe (2011). Clearance rates are unsaturated rates on prey of near optimal size. ESD is the equivalent spherical diameter of the zooplankter. For the purpose of comparison, the ESD and equivalent body volume of jellyfish with an inflated volume were computed from their body carbon and as if they had a carbon density similar to that of other zooplankters (10^5 g C m^{-3}). The predicted values are for zooplankters of lengths L = 0.03 mm, 0.3 mm, 1.0 mm, and 2.5 mm and the predictions are based on default values of all parameters.

Table 1. Sensitivity analyses. Predicted body-volume specific clearance rates ($\times 10^6$ d^{-1}) for a L = 1 mm zooplankter using default input parameters (see electronic supplementary material, appendix A1) and input parameters varying by 1 or 2 orders of magnitude relative to the default. Predictions are reported for scenarios with only rheotactic or only visual/tactic predators and assuming excess densities ($\Delta\rho$) of 5 or 99 kg m^{-3} for the latter.

Parameter	Deviation from default value	Rheotactic	Visual, $\Delta\rho$ = 5 kg m^{-3}	Visual, $\Delta\rho$ = 99 kg m^{-3}
Default	-	1.91	3.36	15.7
Zooplankton food concentration, e	$\times$ 10	0.425	6.59	15.6
	$\times 10^{-1}$	3.62	1.15	15.5
Basal metabolism, M_b	$\times$ 10	2.54	3.57	15.8
	$\times 10^{-1}$	1.91	3.36	15.7
Detection radius of visual predator, R	$\times$ 10	-	3.00	15.5
	$\times 10^{-1}$	-	4.62	18.6
Detection radius of hovering zooplankter, $R_{hovering}$	$\times$ 3	3.80	4.33	45.5
	$\times 3^{-1}$	1.54	3.06	6.58
Detection radius of cruising zooplankter, $R_{swimming}$	$\times$ 3	18.2	93.2	74.1
	$\times 3^{-1}$	1.19	0.80	15.1
Fluid velocity threshold for prey detection in rheotactic predator, U^*	$\times$ 3	4.16	-	-
	$\times 3^{-1}$	1.09	-	-
Predator swimming velocity, v	$\times$ 3	1.10	4.27	17.3
	$\times 3^{-1}$	2.25	2.56	15.2
Feeding independent background mortality, β	$\times$ 10	4.65	4.20	17.0
	$\times 10^{-1}$	0.492	3.07	15.6
Efficiency of energy conversion, η	$\times$ 10	2.25	9.90	15.8

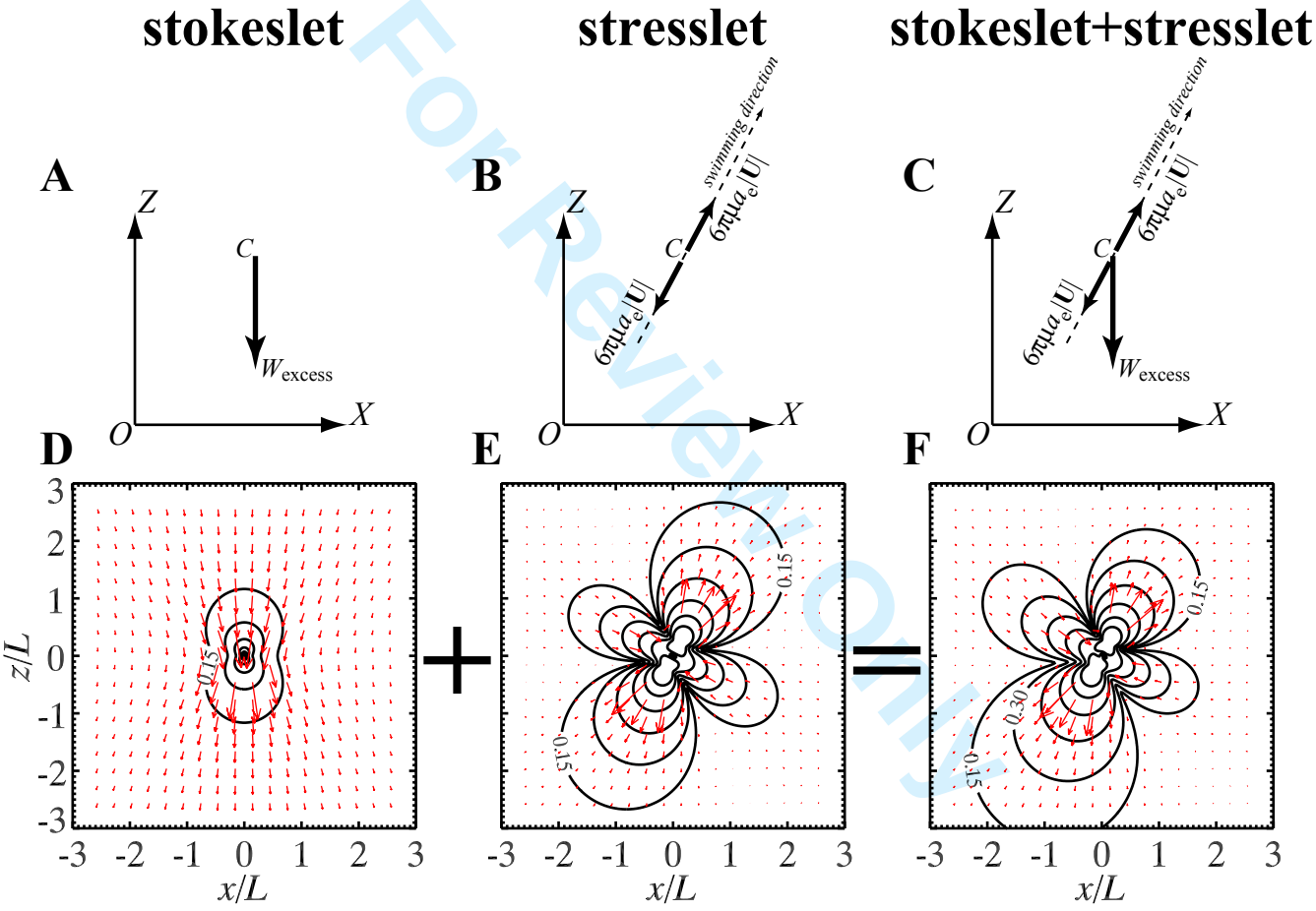

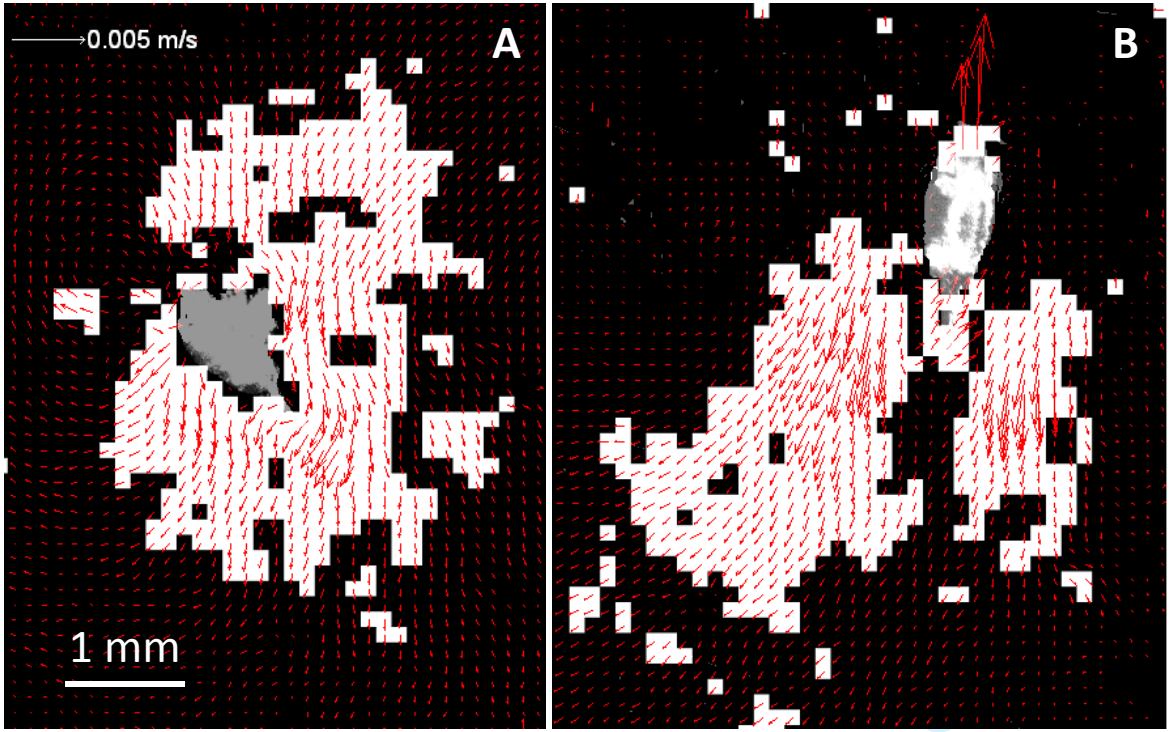
0.005 m/s
A
B
1 mm

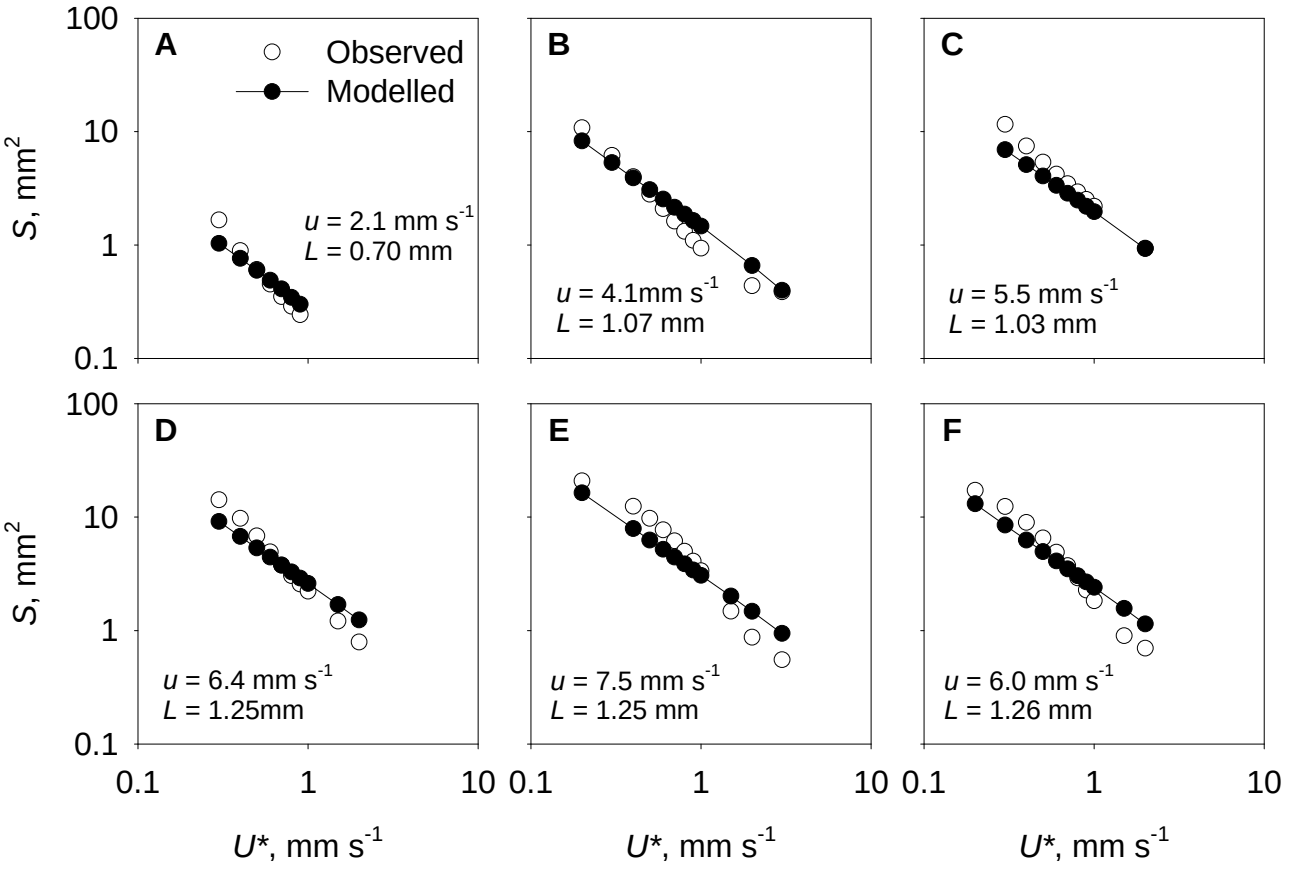
A
Observed
Modelled
u = 2.1 mm s-1
L = 0.70 mm
B
u = 4.1mm s-1
L = 1.07 mm
C
u = 5.5 mm s-1
L = 1.03 mm
D
u = 6.4 mm s-1
L = 1.25mm
E
u = 7.5 mm s-1
L = 1.25 mm
F
u = 6.0 mm s-1
L = 1.26 mm
S, mm2
U*, mm s-1
100
10
1
0.1
0.1
1
10

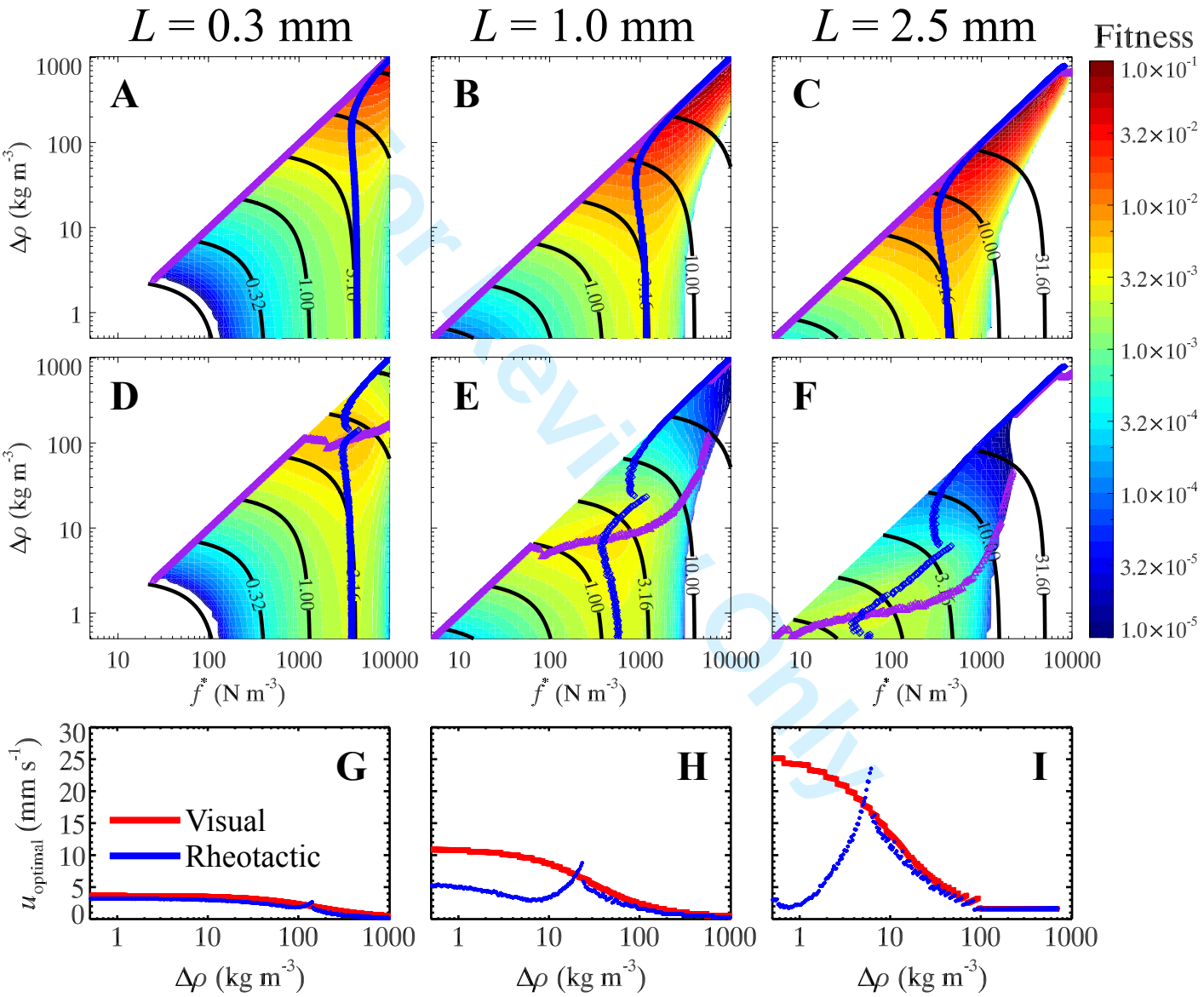

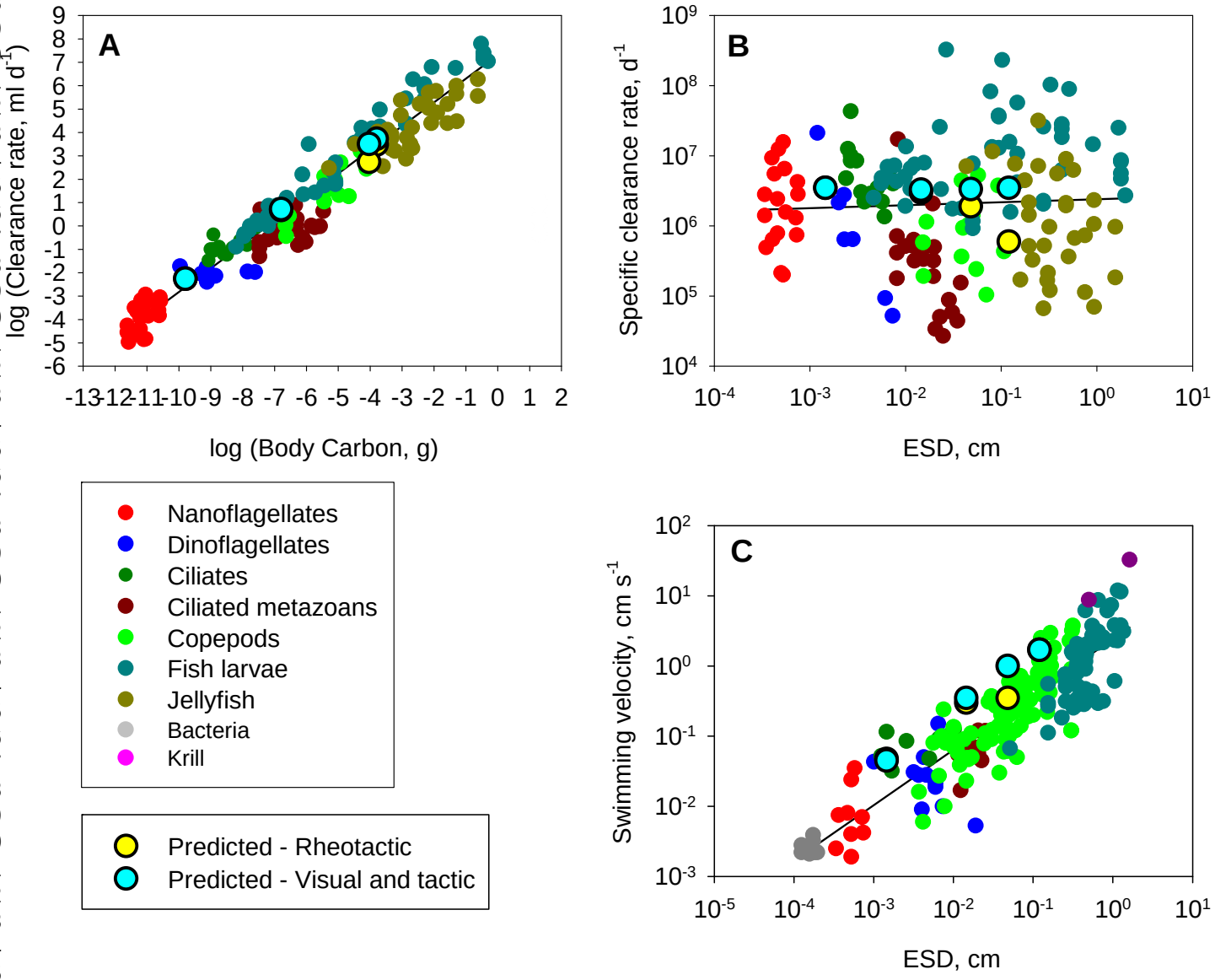
A
log (Clearance rate, ml d-1)
log (Body Carbon, g)
B
Specific clearance rate, d-1
ESD, cm
C
Swimming velocity, cm s-1
ESD, cm
Nanoflagellates
Dinoflagellates
Ciliates
Ciliated metazoans
Copepods
Fish larvae
Jellyfish
Bacteria
Krill
Predicted - Rheotactic
Predicted - Visual and tactic